Materials and Design 195 (2020) 109036

Contents lists available at ScienceDirect

Materials and Design

journal homepage: www.elsevier.com/locate/matdes

Enhancing giant magnetocaloric effect near room temperature by inducing magnetostructural coupling in Cu-doped MnCoGe

S.K. Pal [a,*,1], C. Frommen [a], S. Kumar [b], B.C. Hauback [a], H. Fjellvåg [b], G. Helgesen [a,*]

[a] Institute for Energy Technology (IFE), Instituttveien 18, 2007 Kjeller, Norway
[b] Nanostructures and Functional Materials (NAFUMA), Department of Chemistry, University of Oslo, Sem Sælands vei 26, 0371 Oslo, Norway

HIGHLIGHTS

- Enhanced giant magnetocaloric effect is achieved due to an efficient magnetostructural coupling in $Mn_{1-x}Cu_xCoGe$ compounds.
- Very large magnetic entropy change of 58 $J.kg^{-1}.K^{-1}$ @ $\mu_0H = 5$ T is obtained near room temperature for $Mn_{0.89}Cu_{0.11}CoGe$.
- An excellent effective refrigerant capacity of 258.2 $J.kg^{-1}$ is achieved.
- Wide temperature window (~100 K) is obtained for giant magnetocaloric effect in $Mn_{1-x}Cu_xCoGe$.

GRAPHICAL ABSTRACT

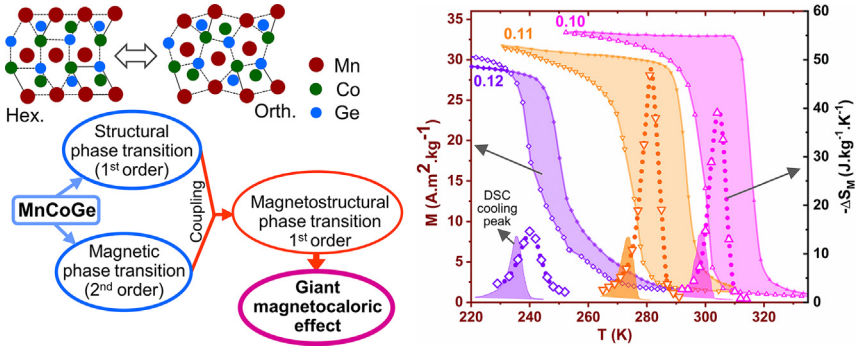

ARTICLE INFO

Article history:
Received 15 May 2020
Received in revised form 26 July 2020
Accepted 3 August 2020
Available online 05 August 2020

Keywords:
Magnetostructural coupling
Giant-magnetocaloric effect
Magnetic cooling
First-order phase transition

ABSTRACT

High performance magnetocaloric materials are crucial to realize the energy efficient and environment friendly magnetic cooling/refrigeration technology. We have designed $Mn_{1-x}Cu_xCoGe$ compounds possessing a giant magnetocaloric effect near room temperature. The magnetic and structural degree of freedom have been coupled by substituting Cu for Mn leading to a first-order magnetostructural phase transformation resulting in a giant magnetocaloric effect over a wide temperature window of 100 *K* (250–350 *K*). A very large entropy change value of 58 $J.kg^{-1}.K^{-1}$ corresponding to a magnetic field change of 5 *T* near room temperature has been obtained for $Mn_{0.89}Cu_{0.11}CoGe$ exhibiting a maximum effective refrigerant capacity of 258.2 $J.kg^{-1}$. The first-order magnetostructural phase transformation which is essential for the giant magnetocaloric effect has been confirmed by a combinatorial master-curve and Arrott-plot analyses. The results of giant magnetocaloric effect realized in $Mn_{1-x}Cu_xCoGe$ are comparable to or better than that of the other reported high performing materials, and this material can be of significant importance for the development of environment friendly and energy efficient cooling devices. The approach of magnetostructural coupling by tuning the structural and magnetic transitions for a giant magnetocaloric effect can also be adopted for other materials to design the best solid-state magnetic refrigerant.

1. Introduction

Serious environmental consequences of the traditional vapor-compression cooling techniques have turned the research efforts towards the development of alternative cooling techniques. The magnetocaloric effect (MCE), a phenomenon that shows temperature

* Corresponding authors.
E-mail addresses: skpal099@gmail.com (S.K. Pal), geir.helgesen@ife.no (G. Helgesen).
[1]Present address: Department of Materials Science and Engineering, Indian Institute of Technology Kanpur, Kanpur, India.

https://doi.org/10.1016/j.matdes.2020.109036

change of a magnetic material upon application/removal of a magnetic field, can be applied for the development of environment friendly magnetic cooling devices for domestic, as well as, commercial purposes. [1–4] The search for new magnetic materials or improving the properties of existing ones exhibiting large MCE near room temperature (RT) is a field of intense research for magnetic cooling technology. It has been demonstrated that the MCE of a magnetic material can be significantly improved by combining the structural degree of freedom with the magnetic one, which can be achieved by tuning the material for a concomitant magnetic and structural transformation. [5–9] The coupling of magnetic and structural degrees of freedom produces a first-order magnetostructural transformation, which in turn leads to a giant magnetocaloric effect.

The magnetic MM'X (M, M' = transition metals, X = p-block element) type equiatomic compounds have received considerable research interest in the past few years because of their remarkable magneto-responsive properties. [8,10–14] MnCoGe is one such important MM'X compounds exhibiting a martensitic structural and a ferromagnetic transformation separated by approximately 100 *K*. The pristine equiatomic MnCoGe compound transforms structurally from high temperature Ni_2In-type hexagonal structure (space group $P6_3/mmc$, #194) to low temperature TiNiSi-type orthorhombic structure (space group Pnma, #62) at approximately 500 *K*. A schematic of hexagonal and orthorhombic crystal structures is shown in Fig. 1(a). Both the hexagonal austenite and the orthorhombic martensite phases are ferromagnetic (FM) in nature with Curie temperatures of $T_C^A = 275$ *K* and $T_C^M = 355$ *K*, respectively. [15,16] Interestingly, the orthorhombic phase possesses a slightly higher saturation magnetization ($\approx 3.86\ \mu_B/f.u.$) than the hexagonal phase ($\approx 2.58\ \mu_B/f.u.$). [17] As the martensitic structural transformation temperature ($T_{str.}$) is higher than the magnetic transition temperature of the martensite (T_C^M) and the austenite (T_C^A) phases, the structural transformation takes place in the paramagnetic (PM) region. In the case when $T_{str.}$ is just below T_C^M, the structural transformation would occur in the FM state and the material would transform directly from PM-austenite to the high-moment FM-martensite phase. This would lead to a magnetostructural coupling and thus a large change in the magnetization could be realized during the magnetostructural transformation (MST).

The tuning of the magnetic and structural transition temperatures of MnCoGe compounds can be achieved *via* application of physical and/or chemical pressures. Some efforts have been made to coincide the structural and magnetic transition temperatures by means of elemental substitution and vacancies at various sites. [18–27] Recently, Aryal *et al.* [28] reported on Ag substitution for Mn in MnCoGe leading to a maximum entropy change of 22 $J.kg^{-1}.K^{-1}$ at 308 *K* for a field change of 5 Tesla (*T*). Substitution of 2 *at.%* Fe for Mn has been shown to produce large refrigerant capacity (212 $J.kg^{-1}$), however the maximum entropy change was quite low (10 $J.kg^{-1}.K^{-1}$). [29] Ma *et al.* [30] reported an entropy change value of 8 $J.kg^{-1}.K^{-1}$ at 260 *K* for a field change of 1 *T* in $Mn_{1-x}Cu_xCoGe$ synthesized by melt spinning methods. However, only the intermediate range of the compositions were investigated, and the nature of the phase transformation in the coupled region has remained elusive. Additionally, the entropy change was calculated only from the continuous magnetic isotherm measurement, which is reported to overestimate the magnetic entropy change values. [31] We have performed the substitution of Cu for Mn in MnCoGe to establish a first-order magnetostructural phase transition by tuning the structural and magnetic transition temperatures. The present study is focused on gaining better understanding of the magnetostructural phase transition and giant MCE in $Mn_{1-x}Cu_xCoGe$ compounds.

Here, we present a systematic and extensive investigation of the structural and magnetic phase transformations in the full range of interesting compositions covering un-coupled, coupled and de-coupled regions in MnCoGe compounds obtained by partial substitution of Cu for Mn. The giant MCE values have been determined following the discontinuous (loop) method which provides a more accurate values for first-order phase change materials. For the first time we have observed a magnetic field induced magnetostructural transformation in $Mn_{1-x}Cu_xCoGe$ compounds. The large (~9 *K*) shift of magnetostructural transition temperature upon a field chage of 5 *T* makes $Mn_{1-x}Cu_xCoGe$ compounds promising for sensor applications. Additionally, for the first time we analyzed the nature of magnetostructural phase transition adopting a combinatorial approach of qualitative universal entropy curve and Arrott plot methods, and the quantitative exponent method to confirm the first-order nature of the magnetostructural phase transition in $Mn_{1-x}Cu_xCoGe$ compounds. The magnetostructural coupling leads to a first-order phase transformation for Cu concentrations in the range of 9–12 *at.%*, and thus results in a giant MCE in wide temperature window of 100 *K*. A phase diagram has been deduced based on the results of calorimetry and magnetic measurements. The approach of designing MnCoGe compound possessing first-order magnetostructural phase transition has been successful in obtaining a large magnetic entropy change and a giant MCE, and also provides a better understanding of Cu substituted MnCoGe compounds. This study paves the way towards designing magnetic materials possessing large magnetic entropy change and giant MCE for the realization of energy efficient and environment friendly magnetic cooling devices.

2. Materials and methods

$Mn_{1-x}Cu_xCoGe$ (x = 0–0.15) compounds were prepared by arc-melting of metal elements Mn, Cu, Co, Ge of purity 99.99 *wt%* or higher under argon gas atmosphere. The arc-melted ingots were sealed in evacuated quartz ampoules and homogenized at a temperature of 1123 *K* for 100 h and then subsequently furnace-cooled to RT. Ingots were cleaned by grinding away the impurities on the surfaces. RT X-ray diffraction (XRD) measurements were performed on powder samples for structural characterization using a Bruker D8 Advance diffractometer with Cu-K_α radiation. Phase matching and structural refinements were carried out using the FullProf/WinPLOTR suite. [32] Temperature dependent structural transformation was studied using a differential scanning calorimetry (DSC 25 – TA Instruments) with a heating/cooling rate of 5 *K*/min. A Quantum Design physical property measurement system (QD-PPMS) was employed to measure isofield (M-T) and isothermal (M-H) magnetization curves. M-T measurements were performed with a temperature step of 2 *K* and a heating or cooling rate of 2 *K/min.*, adopting the settle mode for settling of the temperature. The magnetic field was set in persistant mode providing a stable field for M-H measurements. The field was changed at intervals of 0.02 and 0.2 T in 0–1 *T* and 1–9 *T* ranges, respectively. The magnetization curves were not corrected for demagnetizing field due to the irregular shape of the sample and the powder particles. The magnetic entropy change was evaluated from M-H curves using the integral form of Maxwell's relation following the discontinuous (or loop) method as described elsewhere. [31] In the loop process, when measuring isotherms in the cooling run, the sample is always heated to a fixed temperature in paramagnetic state after each isotherm measurement and then cooled down to the desired measuring temperature. This process erases the history of the sample and the magnetic response remains unaffected by the coexistence of the mixed para- and ferro-magnetic phases. [31] Refrigerant capacity of the compounds was determined by adopting method described by Wood and Potter [33] Effective refrigerant capacity was deduced by deducting the magnetic hysteresis loss from the refrigerant capacity.

3. Results and discussions

3.1. Structural transition

Fig. 1(b) depicts the powder XRD patterns of $Mn_{1-x}Cu_xCoGe$ recorded at RT. It is evident that these compounds crystallize in orthorhombic structure for Cu concentration $x \leq 0.07$. A minor trace of the

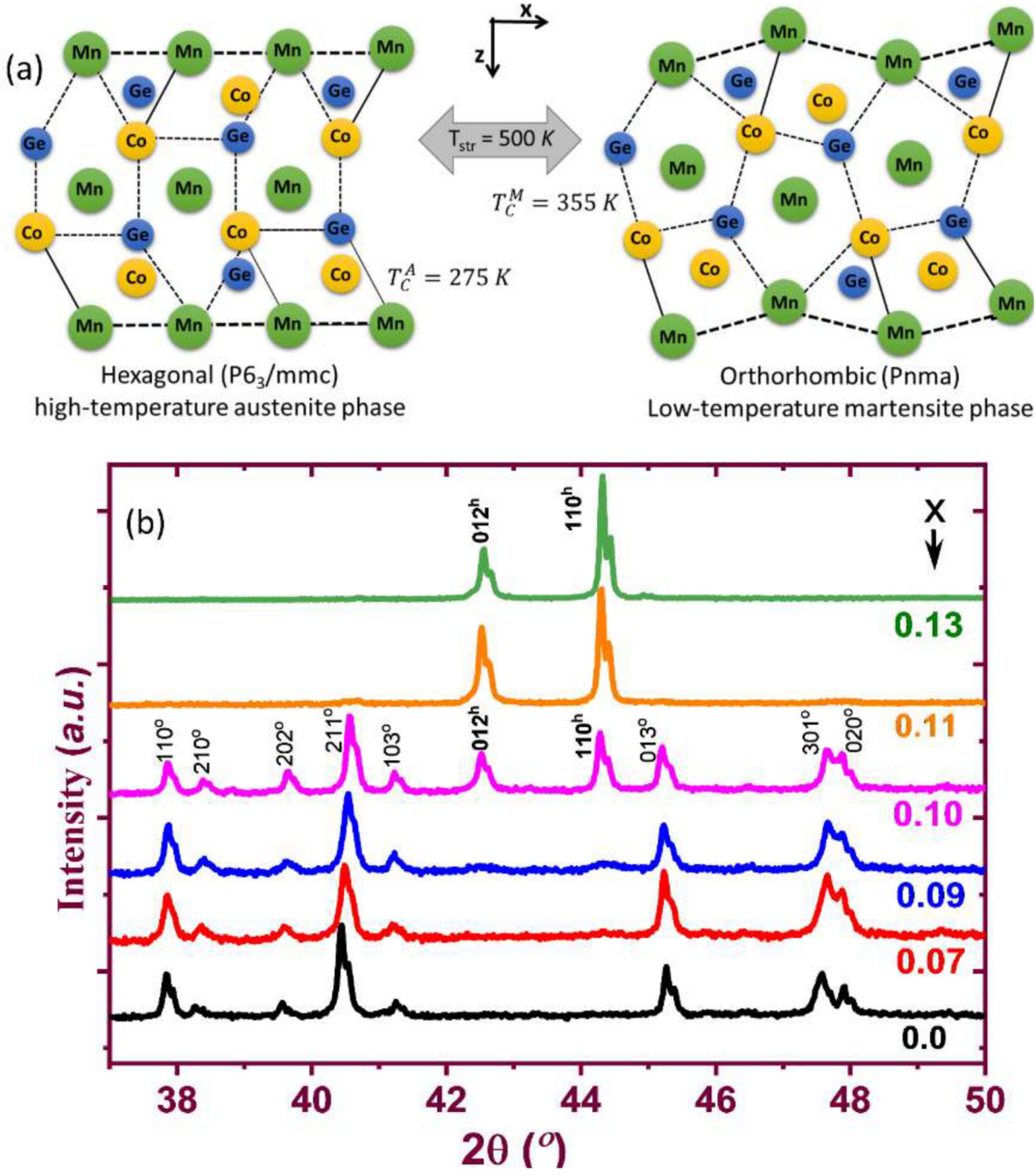

Fig. 1. (a) Hexagonal (Ni_2In-type) and orthorhombic (TiNiSi-type) modifications of the crystal structure of MnCoGe. Atoms at z = ¾ are connected by lines, atoms at z = ¼ are unconnected, (b) room temperature powder XRD patterns of $Mn_{1-x}Cu_xCoGe$ compounds. hkl^o and hkl^h denote the Miller indices for the orthorhombic and the hexagonal structures, respectively.

high-temperature hexagonal phase starts appearing at $x = 0.09$, which then develops to around 35 and 90 *vol%* for $x = 0.10$ and 0.11, respectively. The $Mn_{1-x}Cu_xCoGe$ compounds completely transform to a hexagonal structure for $x \geq 0.12$. This indicates that the substitution of Cu for Mn in MnCoGe can effectively alter the phase stability, and that the hexagonal structure is stabilized at lower temperatures with increasing Cu concentration. The amount of Cu ($x = 0.09$) required for the stabilization of the hexagonal phase at RT is much higher than that reported by Ma *et al.* [30], wherein, a very small amount of Cu ($x = 0.02$), was enough to completely transform the orthorhombic structure to hexagonal at RT. This large difference in *x* values could probably have been due to different synthesis method used. Melt spinning could produce a very different microstructure and the melt-spun ribbons could be inhomogeneous in composition. As can be seen in Fig. 1(b), the Bragg peaks shift towards higher 2θ values with increasing Cu concentration, indicating a lattice contraction of both orthorhombic and hexagonal phases. A reduction of the cell volume is expected since Cu ($r_{Cu} \approx 1.28$ Å) is smaller in size compared to Mn ($r_{Mn} \approx 1.30$ Å). [34] A cell volume change of ~3.9 *vol%* was obtained due to transformation from orthorhombic to hexagonal phase at RT, indicating a significant amount of lattice distortion during the transformation. As the structural transformation in MnCoGe takes place through atomic displacements, an alteration of

the interatomic distances by substitution with smaller size elements would induce negative chemical pressure, similar to the physical pressure effects studied by Caron *et al.* [35] and Wu *et al.* [22], which in turn would facilitate the transformation towards lower temperature.

DSC measurements were carried out to study the temperature dependent structure transformation of various samples. Fig. 2(a) shows DSC thermograms of different samples obtained in heating and cooling cycles in the selected temperature range. It is evident that the structural transformation temperature decreases continuously with increasing Cu concentration. Reduction in peak broadenings with an increase in x up till $x = 0.10$ indicates a faster transition and also suggests that the chemical pressure due to the substitution of Cu for Mn facilitates atomic displacements. The increased peak broadening for $x = 0.13$ could be due to the fact that atomic movement gets sluggish because of the reduced thermal energy at low temperatures. The full temperature range DSC curves for $x = 0.07$ in Fig. 2(b) depict two types of transitions. The weak and broad transition at 345 *K* corresponds to second-order magnetic transition (Curie temperature, T_C), and the strong transitions in the temperature range 360–430 *K* correspond to the martensitic structural transition temperature, T_{str}. The characteristic temperatures for austenite start (T_A^s), austenite finish (T_A^f) in the heating cycle and martensite start (T_M^s), martensite finish (T_M^f) in the cooling cycle are indicated in the Fig. 2(b). The much broader peaks with almost zero thermal hystereses indicate the second-order nature of the magnetic transformation. However, the strong peaks with a significant amount of thermal hysteresis at around 450 *K* reveal the first-order nature of the martensitic transformation.

3.2. Magnetic transition

Temperature dependent magnetization (M-T) curves of selected $Mn_{1-x}Cu_xCoGe$ compounds measured in a magnetic field of $\mu_0 H = 0.1$ *T* are presented in Fig. 3. The shaded peaks represent the heat-flow DSC curves for the cooling cycle. It can be seen that the transition temperature T_C decreases with increasing Cu concentration in the range $x = 0.09$–0.12. The relatively broad magnetic transition without any temperature hysteresis for $x = 0.07$ demonstrates the second-order nature of the PM-FM transition, which is also in agreement with the DSC result discussed earlier. Note that the magnetic transition for $x = 0.07$ is taking place in the orthorhombic phase as is evident from the DSC curve. The M-T curves of $x = 0.09$–0.11 samples show a sharp transition with thermal hysteresis (~20 *K*) indicating the first-order nature of the transition. As it can be seen in case of cooling cycles, the starting point of the magnetic transition (PM-FM) for $x = 0.09$–0.11 coincides with the start of the martensitic transition temperature, T_M^s. The concomitant structural and magnetic transitions lead to the coupling of magnetic and lattice degrees of freedom, which ultimately result in the first-order magnetostructural transformation at T_{MST}. In contrast, the M-T curve of the $x = 0.12$ sample shows a relatively broad start of the magnetic transition at around 260 *K* which then transforms to a sharper transition at a slightly lower temperature. The sharper transition coinciding with the DSC heat-flow curve corresponds to the martensitic transformation, whereas, the broader transition in austenite region corresponds to the Curie temperature of the hexagonal austenite phase. In this case, the magnetic and structural transformations could only be partially coupled as the martensitic transformation starts just before the completion of the magnetic transition. The partial magnetostructural coupling in the $x = 0.12$ is also visible in terms of the narrow temperature hysteresis as compared to that of the $x = 0.09$–0.11 samples. It is of significant importance to note that for the coupled compositions (x = 0.09–0.12), both magnetic and structural transition temperatures decrease at almost the same rate in a wide temperature span (~350–250 *K*), while, the structural transition temperature decreases at a much faster rate than the magnetic one in the composition range beyond $x = 0.09$–0.11. It could be that the magnetic transition temperature (T_C) of the orthorhombic phase is much higher than the transition temperature observed from these M-T curves. However, as the material directly transforms from the PM-hexagonal phase to FM-orthorhombic phase, the magnetic transition is directly mediated by the structural transition until the T_{str} falls below the T_C value of the hexagonal phase. In such a scenario, the material would transform from FM-hexagonal to FM-orthorhombic and hence the magnetic and structure transformations get de-coupled, as seen in the M-T curve of $x = 0.13$ samples.

3.3. Magnetic field induced magnetostructural transformation

A significant change of the magnetization of around 5 $A.m^2.kg^{-1}$ for an applied magnetic field of 0.1 *T*, for $x = 0.13$ sample near the T_{str} indicates that the orthorhombic martensitic phase possesses a higher magnetic moment as compared to that of the hexagonal austenite phase (see Fig. 3). This result is also in agreement with the magnetic moment values of orthorhombic and hexagonal MnCoGe compound reported by

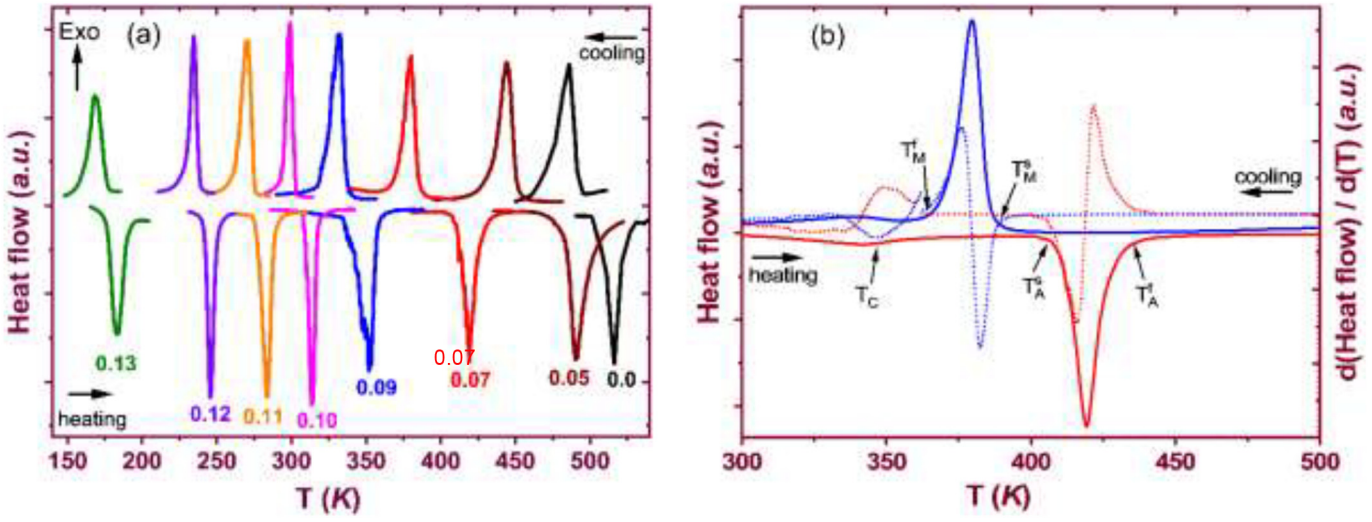

Fig. 2. (a) DSC heat flow curves of $Mn_{1-x}Cu_xCoGe$ as a function of temperature measured at a rate of 5 K/min during heating and cooling cycles, (b) full DSC heat flow curve for x = 0.07 sample. The faint-dotted curve in (b) represents the derivative of the heat flow curve with the zoomed-in region around T_C. T_A^s - austenite start temperature, T_A^f - austenite finish temperature, T_M^s - martensite start temperature, T_M^f - martensite finish temperature.

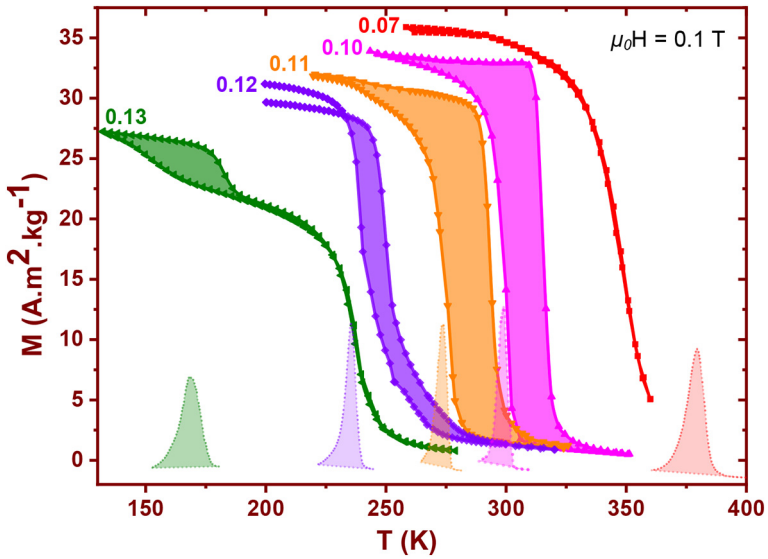

Fig. 3. Temperature dependent magnetization curves of $Mn_{1-x}Cu_xCoGe$ compounds for (a) x = 0.07–0.13 measured in heating and cooling cycles under a magnetic field of 0.1 *T*. The bottom shaded peaks represent the corresponding DSC heat-flow curves measured during the cooling process.

Bazela *et al.* [36] The higher magnetic moment of the martensitic phase is expected to drive T_{str} towards higher temperature in the presence of a magnetic field. In this respect, the M-T curves for the $x = 0.11$ sample showing the magnetostructural transformation near RT were measured at various fields, and are shown in Fig. 4. The M-T curves clearly demonstrate a field induced magnetostructural transformation with the transition temperatures of T_{MST} = 278.8, 281.2, 283.7 and 287.8 *K* corresponding to the applied magnetic fields of 0.1, 1, 2 and 5 *T*, respectively. An upward shift of the transition temperature of around $\Delta T = 9.0$ *K* was estimated for an applied magnetic field of 5 *T*. The shift of the martensitic transition temperature can be attributed to the difference in Zeeman energy of the austenite and the martensite phases under the stronger applied magnetic fields. This difference in energy can enhance the stability of the martensitic phase and hence change the equilibrium temperature, leading to a magnetic field induced martensitic transformation. [37] The change of the martensitic transformation temperature (ΔT) induced by magnetic field changes (ΔB) is approximately given by the Clausius–Clapeyron relation

$$d(\mu_0 H)/dT = \Delta S/\Delta M \text{ or } \Delta T \approx (\Delta M/\Delta S)\Delta(\mu_0 H) \quad (1)$$

where, T is the absolute temperature, μ_0H is the applied magnetic field, and ΔM and ΔS are the differences in magnetization and entropy, respectively, between the parent austenite and the martensite phases. Substituting ΔM ($=M^{mar.}_{\mu 0H=5T} - M^{aus.}_{\mu 0H=0T} \approx 77\ A.m^2.kg^{-1}$) and ΔS ($\approx 47.5\ J.kg^{-1}.K^{-1}$) values corresponding to $\mu_0\Delta H = 5\ T$ estimated from M-T curve (Fig. 4) and the DSC curve (Fig. 2), respectively, for $x = 0.11$ samples, an approximate value of $\Delta T = 8.1$ *K* was calculated, which is also very close to the experimentally determined ($\Delta T = 9.0$ *K*) value.

On the basis of above described experimental results obtained using the magnetometry and the calorimetry investigations, a phase diagram

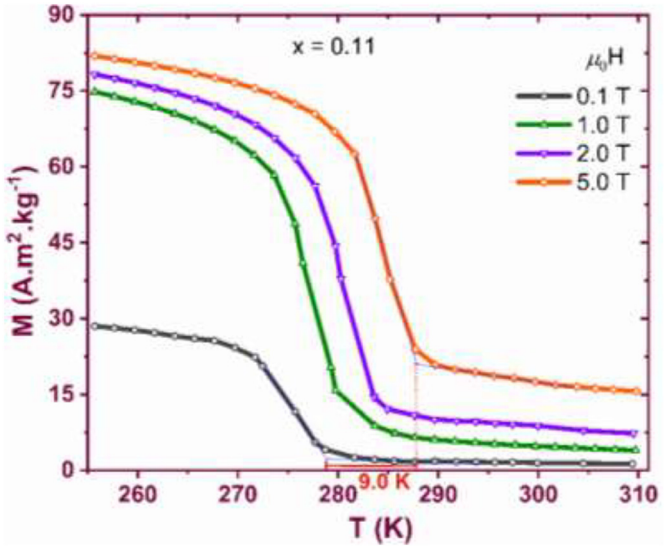

Fig. 4. Temperature dependent magnetization curves of $Mn_{0.89}Cu_{0.11}CoGe$ compound showing magnetic field induced magnetostructural transformation.

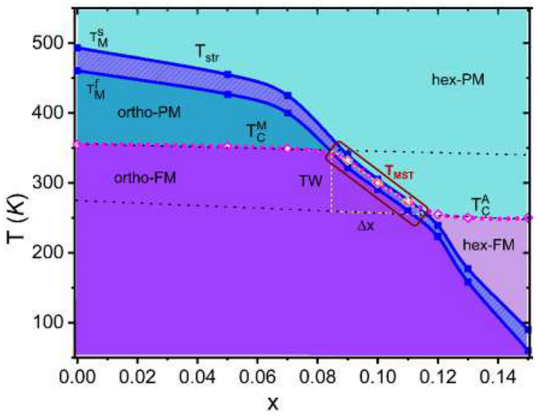

Fig. 5. Magnetic and structural phase diagram of $Mn_{1-x}Cu_xCoGe$ compounds. The dotted magenta curve with open symbols denote the Curie temperature, the upper and lower blue curves with solid squares correspond to the start (T^s_M) and finish (T^f_M) of the martensitic transformation temperature. The upper and lower dashed-black lines represent a trend of the Curie temperatures for the martensitic orthorhombic and the austenitic hexagonal phases, respectively. The highlighted light-yellow region represents the magnetostructural-coupled region (T_{MST}), and TW and Δx denotes the temperature window and the composition region, respectively, for the desired magnetostructural coupling. The graph shows the data measured during the cooling process of the samples. (For interpretation of the references to colour in this figure legend, the reader is referred to the web version of this article.)

of the $Mn_{1-x}Cu_xCoGe$ system for the cooling cycle is presented in Fig. 5. It is demonstrated that the martensitic transformation temperature is continuously lowered by increasing the substitution of Mn by Cu. The magenta colored curve with open symbols corresponding to T_C reveals that Cu substitution for Mn has very little effect on T_C values in both the orthorhombic and the hexagonal regions. This eventually gives the upper (~350 *K*) and lower (~250 *K*) temperature limits of a temperature window of approximately 100 *K*. The dashed-black lines represent a trend line for the Curie temperatures of martensite orthorhombic T_C^M and austenite hexagonal T_C^A phases, respectively. Although, following the trend line the actual Curie temperature of the orthorhombic phase may be higher than the structural transformation temperature, as in the Δx range the material transforms from paramagnetic austenite to ferromagnetic martensite upon cooling. In this case the magnetic transition is directly controlled by the structural transition. The simultaneous occurrence of magnetic and structural transformations can be established within this temperature window (TW), and is highly desired for the magnetostructural coupling in order to realize a giant MCE. The sharp decrease of T_C for $x = 0.09$–0.11 can be ascribed to the structurally driven magnetic transitions leading to the magnetostructural phase transformation.

Magnetic field dependent magnetization (M-H) curves of $x = 0.10$ sample recorded at various temperatures are presented in Fig. 6. The M-H curves were measured while cooling the samples from PM state following the loop process. A linear increase of the magnetization with increasing field for temperatures above 308 *K* ($>T_{str}$) indicates a PM state for the austenite. Interestingly, a sudden change in the slope of the magnetization curves at fields around 7.7, 5.4, 3.6, 2.1 and 0.6 *T* for temperatures 308, 306, 304, 302, and 300 *K*, respectively, can be seen in Fig. 6. However, it is important to note that these temperatures are well above the T_{MST} ($= 298$ *K*) for $x = 0.10$ compound. The increased magnetization and the positive change in the slope of M-H curves indicate the presence of a metamagnetic feature arising from the partial transformation of the austenite phase to the martensite phase due to the application of the magnetic field. This phenomenon demonstrates the field induced martensitic transformation of these materials, which is a confirmation of the same effect observed in terms of the shift of the magnetic transition temperature observed in the M-T curves shown in Fig. (4) for $x = 0.11$ compound. It is also worth noting that the strength of field required for the martensitic transformation decreases with decrease in temperature. This is basically attributed to the increased magnetization and also the reduced thermal energy which induces the martensitic transformation at lower temperatures, requiring less external magnetic energy for the transformation.

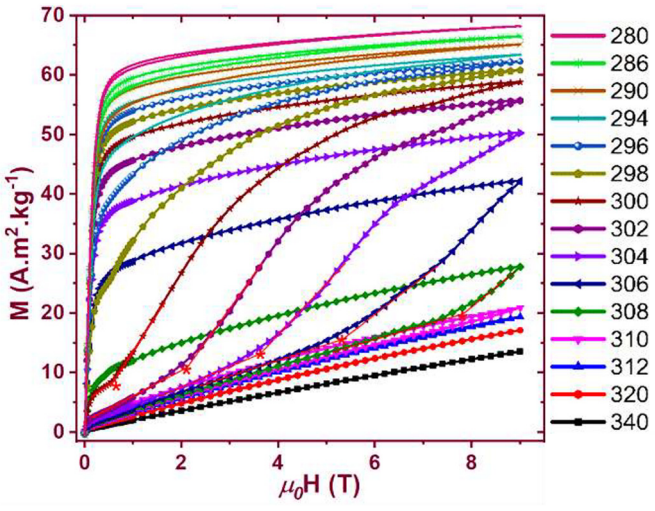

Fig. 6. Isothermal magnetization (M *vs* μ_0H) curves for x = 0.10 compound. The star symbols associated with the tangents to the M-H curves corresponding to selected temperatures denote the field required for the martensitic transformation.

3.4. Giant-magnetocaloric effect

MCE was determined through the isothermal magnetic entropy changes (ΔS_M) which were calculated from the M-H curves using the integral form of the Maxwell's relation;

$$\Delta S_M(T,H) = \mu_0 \int_0^H \left(\frac{\partial M(T,H)}{\partial T}\right)_H dH \quad (2)$$

As the compounds show metamagnetic behavior and first-order phase transition, the loop method of M-H curve measurements was adopted for the determination of ΔS_M. In the loop method, the sample is first heated to a complete PM state and then cooled back to the desired measurement temperature in absence of a magnetic field. This method has been proven as a suitable procedure to suppress the effect of coexisting magnetic phases during the phase transition. [31] Fig. 7 shows the thermal variation of $-\Delta S_M$ for selected composition for $Mn_{1-x}Cu_xCoGe$. The maximum $-\Delta S_M$ values of 22, 40, 48 and 15 $J.kg^{-1}.K^{-1}$ for $x = 0.09$, 0.10, 0.11 and 0.12, respectively, were obtained for a field change of 5 *T* during the cooling cycle. The entropy change values were also determined during the heating cycle for comparison. The maximum $-\Delta S_M$ values were obtained as 23, 43, 58 and 16 $J.kg^{-1}.K^{-1}$ for x = 0.09, 0.10, 0.11 and 0.12, respectively. It can be seen that the maximum $-\Delta S_M$ value was significantly increased to 58 $J.kg^{-1}.K^{-1}$ for x = 0.11, whereas the other compositions showed nearly the same maximum $-\Delta S_M$ values during heating and cooling cycles. The maximum $-\Delta S_M$ value of 58 $J.kg^{-1}.K^{-1}$ for $\mu_0\Delta H = 5$ *T* is the highest entropy change value reported to date in the MnCoGe and similar compounds. Moreover, it is found that the entropy change value for $x = 0.11$ compound is comparable to or higher than those of some high-performance RT magnetocaloric materials (see Table 1 for comparison). While the increase on $-\Delta S_M$ value for x = 0.11 during the heating run is not yet fully understood, a sharp first-order transition resulting from an efficient magnetostructural coupling can be responsible for it. Here, 11 *at.%* seems to be the optimal amount of substitution of Cu for Mn providing optimal chemical pressure for a fast kinetics of the magnetostructural phase transition. Moreover, as proposed by A. Diestel *et al.*, [43] in case of a slight chemical inhomogeneity in the sample there will be coexisting regions which would place the system in a non-equilibrium thermodynamics where changes in the martensite transformation nucleation barrier and growth will vary for both heating and cooling cycles. [43] As the entropy variation as a function of temperature is a combination of both applied magnetic field and temperature there will be variations in both martensitic transformation onset temperature as well as the strength of $-\Delta S_M$. In a temperature induced process, the nuclei orientation and all growth directions are equal, whereas, for a field induced process some nuclei and growth directions are preferred over others. The fast kinetics of martensitic transformation might be preferred during heating cycle in applied magnetic field leading to a slight increase in the $-\Delta S_M$ value.

The entropy change values were also determined from the DSC heat flow curves (Fig. 2 (a)) measured during heating and cooling cycles in absence of applied magnetic field. Total entropy change corresponding to the structural transition were obtained to be 40.7, 48.1, 49.4 and 45.7 $J.kg^{-1}.K^{-1}$ during cooling and 43.7, 51.0, 53.5 and 46.1 $.kg^{-1}.K^{-1}$ during heating cycle for x = 0.09, 0.10, 0.11 and 0.12, respectively. Some discrepancy between the entropy change values determined from the DSC heat flow measurement and isothermal M-H curves is obvious as these are two different techniques and the material is cycled differently during each measurement. Nevertheless, the maximum $-\Delta S_M$ values obtained from both DSC and M-H curves follow the same trend. Similar difference in $-\Delta S_M$ values obtained from DSC (33.4, 42.5 $J.kg^{-1}.K^{-1}$) and M-H curves (9.4, 22 $J.kg^{-1}.K^{-1}$) for various (5,

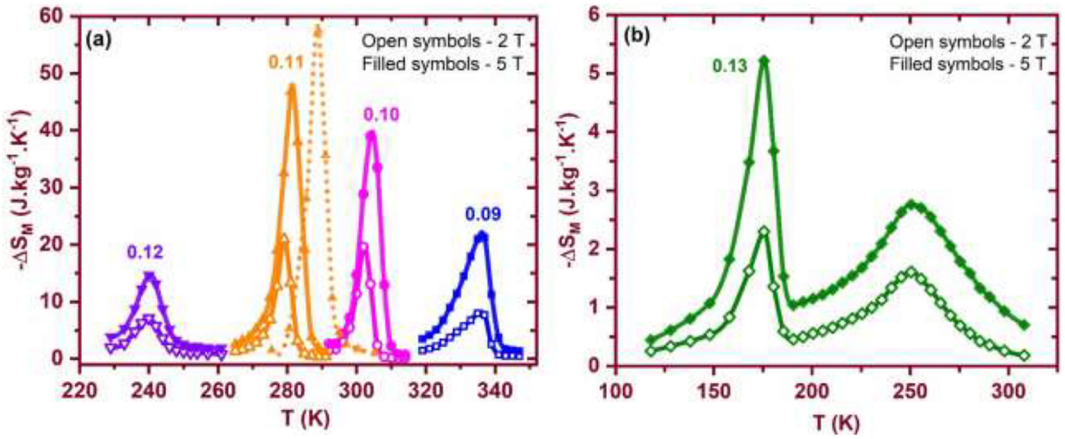

Fig. 7. Magnetic entropy changes derived from isothermal magnetization curves of $Mn_{1-x}Cu_xCoGe$ compounds for (a) x = 0.09–0.12, and (b) x = 0.13. The dotted line curve represents the entropy change during heating cycle and the remaining curves correspond to entropy change measured during the cooling cycle.

6 *at.%*) Ag doped MnCoGe compounds were also reported by Aryal *et al.* [28].

Normally, an asymmetric shape of $-\Delta S_M$ *vs* T curve is observed for first-order phase transition materials. The extent of asymmetry varies with the material. Looking at Fig. 7 (a), the asymmetry can be clearly seen in x = 0.09 curve. There is some degree of asymmetry in the x = 0.10 and x = 0.11 curves as well; however, less pronounced than that of the x = 0.09 curve which could be attributed to the efficient magnetostructural coupling. Similar low degree of asymmetry has also been observed in MnCoGe system reported by A. Aryal *et al.* and G.J. Li *et al.*, for Ag and Fe doped MnCoGe compounds. [18,28] The sharp $-\Delta S_M$ peaks for the $x = 0.10$ and 0.11 samples demonstrate a strong magnetostructural coupling, while the widening of the $-\Delta S_M$ peak of the $x = 0.09$ sample may be due to a weak coupling. In addition, two separate $-\Delta S_M$ peaks can be seen for $x = 0.13$ sample as shown in Fig. 7(b). The wide peak at around 245 *K* corresponds to the second-order magnetic transition; while, the relatively sharp peak at around 170 *K* corresponds to the martensitic structural transition which is of first-order in nature. This reveals that in the case of de-coupled state the entropy changes of the individual magnetic and structural contribution are quite small and that the coupling is a must for the giant change in the entropy of the compounds.

Refrigerant capacity (RC) is another important property of magnetocaloric materials, which represents the amount of heat transferred during one thermodynamic cycle. RC values of the selected compounds were calculated following the method proposed by Gschneider *et al.* [44] which is basically the area under the $-\Delta S_M$ peak in the temperature range of the full width at half maxima (FWHM) of the peak. The RC is given by the following expression [33],

$$RC_{FWHM} = \int_{T_1}^{T_2} \Delta S_M(T)dT \tag{3}$$

where T_1 and T_2 correspond to the lower and upper temperatures at the FWHM of $-\Delta S_M$ peak. Thus, for a large RC, the material is expected to have a high $-\Delta S_M$ value and a wide transition region (*i.e.* broad $-\Delta S_M$ peak). The RC_{FWHM} values of 236.5, 273 and 332.5 $J.kg^{-1}$ were obtained for $x = 0.09$, 0.10 and 0.11 samples, respectively. As the temperature span at FWHM ($\delta T_{FWHM} = T_2\text{-}T_1$) was relatively small with values of 11, 7 and 7 *K* for the $x = 0.09$, 0.10 and 0.11 samples, respectively, which is normally the case for first-order phase transition materials, these large RC values are basically attributed to the high $-\Delta S_M$ values.

Magnetic hysteresis is known to adversely affect the refrigerant capacity of magnetocaloric materials. A significantly large hysteresis can be seen in the M-H curves (Fig. 6) near the magnetostructural transition temperature arising basically due to the metamagnetic behavior of the first-order transition. Such hysteresis causes energy loss referred as hysteresis loss (E^{hys}) during magnetic field cycling resulting in a reduction of the refrigerant capacity of the magnetocaloric materials. The effective refrigerant capacity (ERC) was deduced by deducting the maximum E^{hys} from RC value obtained from $-\Delta S_M$ *vs* T curve. ERC values of 200.9 $J.kg^{-1}$ and 258.2 $J.kg^{-1}$ for a magnetic field change of 5 T and 354.8 $J.kg^{-1}$ and 401 $J.kg^{-1}$ for a magnetic field change of 9 T were obtained for x = 0.10 and 0.11 compounds, respectively.

Table 1
Magnetocaloric properties of the materials of present work and some other interesting materials.

Materials	$-\Delta S_M$ ($J.kg^{-1}.K^{-1}$) at $\mu_0\Delta H = 2$ *T*	$-\Delta S_M$ ($J.kg^{-1}.K^{-1}$) at $\mu_0\Delta H = 5$ *T*	T_{pk} (*K*)	ΔT_{FWHM}	Reference
$Mn_{0.91}Cu_{0.09}CoGe$ cooling (heating) cycle	8 (9)	21.5 (23)	336	11	Present work
$Mn_{0.90}Cu_{0.10}CoGe$ cooling (heating) cycle	19.5 (22)	39 (43)	304	7	Present work
$Mn_{0.89}Cu_{0.11}CoGe$ cooling (heating) cycle	21 (24)	47.5 (58)	281	7	Present work
$Mn_{0.88}Cu_{0.12}CoGe$ cooling (heating) cycle	7 (8)	14.6 (16)	240	9.5	Present work
MnCoGe	3.1	5.8	343	50	[19]
$Mn_{0.665}CoGe$	10	25.5	289	10	[16]
$MnCo_{0.94}Fe_{0.06}Ge$	12	27.5	316	6	[18]
$Mn_{0.94}Ti_{0.06}CoGe$	4.5	14.8	235	–	[38]
$Mn_{0.96}Cr_{0.04}CoGe$	11	28.5	322	10	[39]
$Mn_{0.94}Ag_{0.06}CoGe$	9	22.0	274	12	[28]
$MnFeP_{0.45}As_{0.55}$	8	18	305	20	[40]
$La(Fe_{0.89}Si_{0.11})_{13}H_{1.3}$	24	28	291	22	[41]
$Gd_5Si_2Ge_2$	27	36.4	277	–	[42]

Magnetic entropy changes for magnetic field change of 0–2 T and 0–5 T, temperature corresponding to peak entropy change (T_{pk}), and full width at half maxima temperature (ΔT_{FWHM}) of the entropy change curve.

The substitution of Cu for Mn in MnCoGe has been successful in achieving a large magnetic entropy change and refrigerant capacity by coupling the magnetic and lattice degrees of freedom which leads to a significant improvement in the giant MCE. However, the large thermal hysteresis present in the magnetostructurally coupled $Mn_{1-x}Cu_xCoGe$ compounds (x = 0.09–0.12) can be an issue in direct application of these materials for magnetic refrigeration. Nevertheless, there is scope for further optimization of these materials by appropriate elemental doping or applying physical pressure to improve the reversibility by decreasing thermal hysteresis. [21,45,46]

Increasing Cu content in $Mn_{1-x}Cu_xCoGe$ leads to a rapid decrease of the structural transition temperature because of the induced negative chemical pressure due to smaller size of Cu as compared to that of Mn. It is important to note that only a slight decrease in the magnetic transition temperature (Curie temperature) takes place due to Cu substitution for Mn unlike the case of Cu substitution for Co which results in fast decrease of the Curie temperature as reported by Zhang *et al.* [47]. The slight decrease of the Curie temperature could be attributed to the magnetic dilution of $Mn_{1-x}Cu_xCoGe$ due to the substitution with non-magnetic Cu for magnetic Mn atom. A slow decreasing rate of Curie temperature and faster decreasing rate of structural transition temperature is beneficial for the overlapping of both transitions. The compositions for which the structural transition temperature becomes lower than the magnetic transition temperatures, the magnetic transition would be mediated by the structural transition leading to a first-order magnetostructural phase transition. The decrease of the structural/magnetostructural phase transition temperature of $Mn_{1-x}Cu_xCoGe$ with increasing Cu content could be attributed to the increased *c*/*a* ratio and higher electronegativity of Cu ($\chi_{Cu} = 1.90$) as compared to that of Mn ($\chi_{Mn} = 1.55$). [48]

3.5. First-order magnetostructural phase transformation

The magnetocaloric effect and the magnetic entropy change are closely related to the nature of the phase transition. In general, the second-order phase transition leads to a broader entropy change peak ($-\Delta S_M$ *vs* T curve), whereas, a sharp entropy change peak with high value of maximum entropy change is observed in the case of a first-order phase transition. Different methods have been employed to study the nature of the phase transition through magnetic measurement. [49–51] Arrott plot (M^2 *vs* H/M) in combination with Banerjee criterion has been broadly used to investigate the nature of the phase transitions. [49,52] A second-order magnetic phase transition results in a positive slope of the M^2 *vs* H/M curve in the whole field range, while a negative slope and/or an S-shape of the M^2 *vs* H/M curve would be observed in case of a first-order magnetic phase transition. Arrott plots for $x = 0.10$ compound are shown in Fig. 8(a). The compound with $x = 0.10$ was chosen because of its proximity to RT, and coupled structural and magnetic transitions. A negative slope in the M^2 *vs* H/M curves can be seen for temperatures between 310 and 298 *K*, which also coincides with field-induced magnetostructural transition presented in Fig. 6. According to the Banerjee criterion, negative slope indicates the first-order nature of the magnetostructural phase transition for $x = 0.10$ sample. However, Banerjee criterion which is based on the assumption that the material follows a mean field model, has been reported to provide contradictory results in some specific cases such as $DyCo_2$ and $MnFeP_{0.46}As_{0.54}$. [51,53] Recently, Franco *et al.* [50] proposed an alternative method based on the scaling nature of the entropy change curves ($-\Delta S_M$-T) of second-order phase transformation materials. The universal scaling method has been suggested to be more effective in determining the nature of the phase transformation. The universal curve was constructed by normalizing all $-\Delta S_M$ *vs* T curves with their respective peak entropy change (S_M^{pk}), $\Delta S_M' = \Delta S_M(T)/\Delta S_M^{pk}$ (see Fig. 8(b) and (c)). The temperature axis was rescaled to θ below and above the temperature (T^{pk}) corresponding to the peak entropy change value by imposing the condition that the positions of two reference points in the curve correspond to $\theta = \pm 1$, *i.e.*

$$\theta = \begin{cases} -(T-T_C)/(T_{r_1}-T_C), & T \le T_C \\ (T-T_C)/(T_{r_2}-T_C), & T > T_C \end{cases} \quad (4)$$

Here, T_{r_1} and T_{r_2} are the reference temperatures corresponding to $\frac{1}{2}S_M^{pk}$ and $T_C = T^{pk}$.

The rescaled universal curve of $-\Delta S_M$ for $x = 0.10$ compound is shown in Fig. 8(c). It is well established that all $\Delta S_M'$ *vs* θ curves collapse onto one curve for materials with second-order phase transition. [51] In the present case, the curves collapse within the range of $-1 < \theta < 1$ by the condition of construction, however a significant deviation occurs outside $-1 < \theta < 1$. This break-down in the universal behavior suggests the first-order nature of the phase transition of $x = 0.10$ compound. Moreover, the deviation from the universal curve can be quantified as vertical dispersion of $\Delta S_M'$ values corresponding to $\theta < -1$. [51]

$$dispersion = \frac{W(\theta = -3)}{\Delta S_M'} \quad (5)$$

where, $W(\theta = -3)$ is the width of the vertical spreading $\Delta S_M'$ curve corresponding to $\theta = -3$. A vertical dispersion of 90% was obtained for an arbitrary value $\theta = -3$. It is pointed out that a dispersion of up to 30% can be observed for the second-order phase transition as well, arising probably due to measurement error. Here, the dispersion of 90% is significantly large confirming the first-order nature of the magnetostructural phase transition for $x = 0.10$ compound.

As reported by Law *et al.* the magnetocaloric effect (field and temperature dependence of ΔS_M) can be used to quantitatively determine the order of phase transition. [54] The field dependence of ΔS_M can be represented as power law of the field

$$|\Delta S_M| \propto (\mu_0 H)^n \quad (6)$$

where, n is an exponent, which depends on the field and temperature. The local exponent *n* was calculated by the following relationship:

$$n(T,H) = \frac{d\ \ln(-\Delta S_M)}{d\ \ln(\mu_0 H)} \quad (7)$$

Fig. 8(d) represent a 3D-plot of *n* with respect to field and temperature. It has been reported that for temperatures well below the transition temperature T_{peak}, *n* should have a value that tends towards 1, and for T much larger than T_{peak}, n tends towards paramagnetic value of 2. [55,56] At $T = T_{peak} = T_C$, *n* depends on the critical exponents of the material, reaching a minimum value close to 2/3 for second-order phase transition materials, while an overshoot in n ($n > 2$) is observed at $T = T_{peak}$ in the case of first-order phase transition materials. [50,54] In the present case, as shown in Fig. 8(d), *n* values are close to 1 and 2 for temperatures far below and far above T_{peak}, respectively. However, at $T = T_{peak}$ and in the vicinity, *n* value strongly depends on temperature and field. Nevertheless, *n* is much higher than 2 at $T = T_{peak}$ for all fields, providing a confirmation of the first-order phase transition in $x = 0.10$ compound. Note that Arrott plot and universal curve analysis distinguish the first-order phase transition and second-order phase transition only qualitatively, while the exponent method provides a quantitative determination of the phase transition and therefore it is thought to be more reliable method. Thus, it has been shown using different techniques namely, Arrott plot, universal scaling and exponent method that the nature of the magnetostructural phase transition in $Mn_{1-x}Cu_xCoGe$ is first-order, which ultimately leads to a giant magnetocaloric effect. Additionally, the large thermal hysteresis in M-T curves and structural transition in DSC heat flow curves also indicated the presence of first-order phase transition.

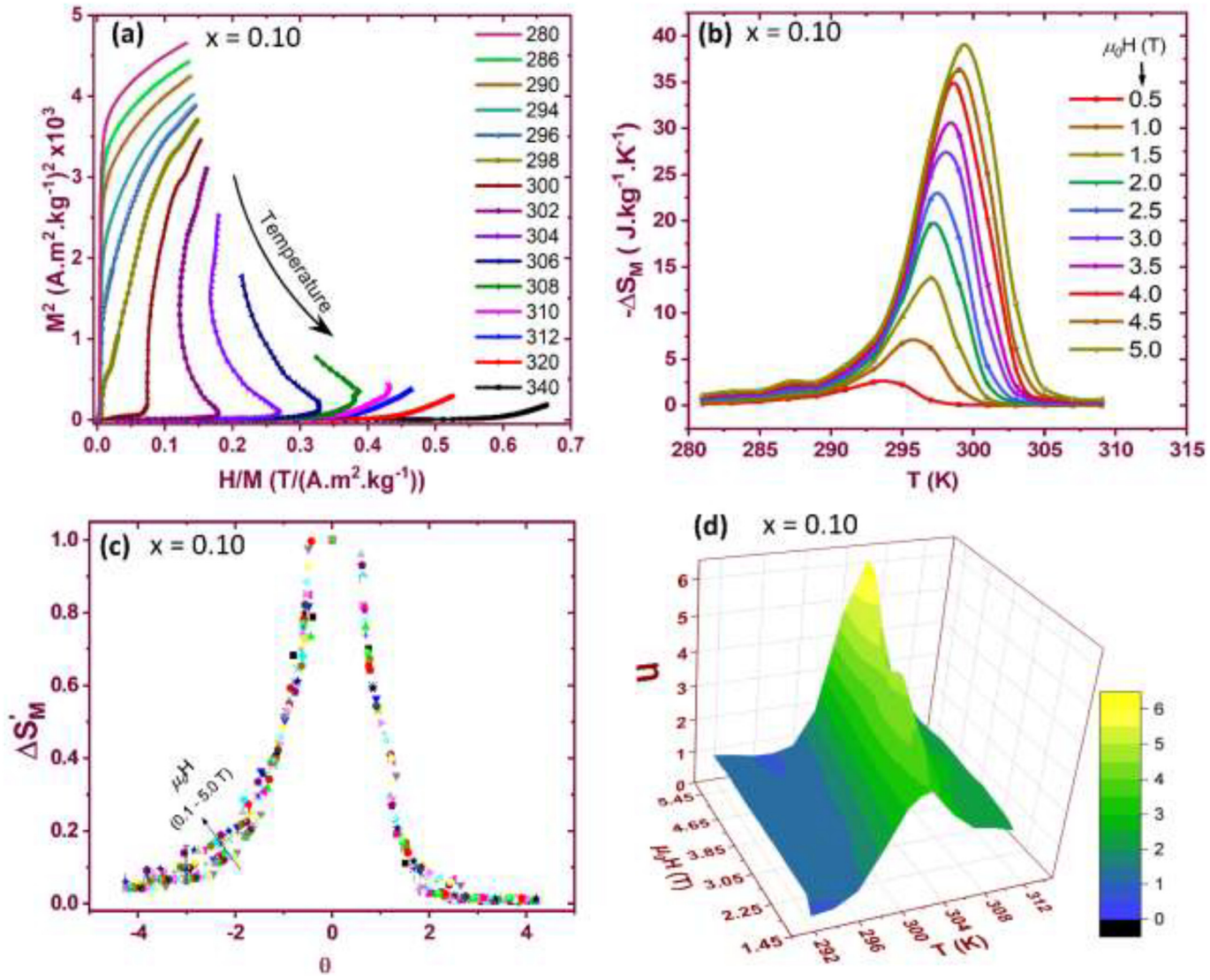

Fig. 8. Thermomagnetic data for the x = 0.10 compound confirming the first-order nature of the magnetostructural transition. (a) Arrott plot having negative slope of M^2 *vs* H/M curves, (b) magnetic entropy changes curve for various fields, (c) universal entropy change curve in field range 0.1–5 T having a dispersion of 90% at θ = 3.0, and (d) 3D plot of exponent, *n* for various field and temperatures showing an overshoot near the transition temperature.

4. Conclusions

A detailed study of the structural and magnetic phase transformations and the magnetocaloric effect was performed on a series of $Mn_{1-x}Cu_xCoGe$ (x = 0.0–0.13) compounds. We demonstrate that the substitution of Cu for Mn is instrumental in establishing a magnetostructural coupling in MnCoGe leading to a very high value of magnetic entropy change. Through tuning Cu content, the first-order magnetostructural transformation occurs in the temperature region where the structural transition temperature lies between the Curie temperatures of both orthorhombic and hexagonal phases. The findings reveal that the materials transform from paramagnetic austenite → paramagnetic martensite → ferromagnetic martensite for compositions $x < 0.08$, and from paramagnetic austenite → ferromagnetic austenite → ferromagnetic martensite for compositions $x > 0.12$ upon cooling. The concomitant structural and magnetic transition occurs in the narrow composition range $x = 0.09$–0.12, where the materials transforms directly from paramagnetic austenite to ferromagnetic martensite leading to a first-order magnetostructural transformation which occurs only when the structural transition temperature lies between the two Curie temperatures. A large separation of the Curie temperatures of two phases offers to a wide temperature window of 100 *K* (250–350 *K*) for the first-order magnetostructural transition in the composition range of $x = 0.09$–0.12. The magnetostructural coupling results in a metamagnetic behavior and a magnetic-field-induced martensitic transformation owing to the difference in Zeeman energy of the austenite and martensite phases. The coupling of the lattice and spin degrees of freedom results in the first-order magnetostructural transformation leading to a giant magnetocaloric effect with a very high value of maximum entropy change of 58 $J.kg^{-1}.K^{-1}$ and effective refrigerant capacity of 258.2 $J.kg^{-1}$ for a field change of 0–5 *T* at ~290 *K* corresponding to composition $x = 0.11$. This is the highest entropy change value reported in MnCoGe system, and also higher or comparable to other high-performance magnetocaloric materials. The tunable crystallographic and magnetoresponsive effects of these compounds along with a giant magnetocaloric effect make them very promising magnetocaloric materials. This study provides a detailed understanding of the first-order magnetostructural transition and giant magnetocaloric effect in $Mn_{1-x}Cu_xCoGe$ compounds, and paves a way towards desigining and tuning materials possesing a giant magnetocaloric effect. The strategic

approach of crystal engineering to enhance the magnetocaloric effect by establishing efficient coupling of the magnetic and structural degrees of freedom can be adopted to design other high-performance magnetocaloric materials for magnetic cooling applications.

Data availability

The data that support the findings of this study are available from the corresponding author upon reasonable request.

Declaration of Competing Interest

The authors declare no competing financial interest.

Acknowledgements

This work was financially supported by the internal grants of Institute for Energy Technology (IFE), Norway. We are thankful to Prof. A. T. Skjeltorp for fruitful discussions and M. H. Sørby for assistance with measurements and device operation.

References

[1] A.M. Tishin, Y.I. Spichkin, The Magnetocaloric Effect and its Applications, CRC Press, 2016.
[2] K.A. Gschneidner Jr., V.K. Pecharsky, A.O. Tsokol, Recent developments in magnetocaloric materials, Rep. Prog. Phys. 68 (6) (2005) 1479–1539, https://doi.org/10.1088/0034-4885/68/6/R04.
[3] E. Brück, Developments in magnetocaloric refrigeration, J. Phys. D. Appl. Phys. 38 (23) (2005) R381–R391, https://doi.org/10.1088/0022-3727/38/23/R01.
[4] V. Franco, J.S. Blázquez, J.J. Ipus, J.Y. Law, L.M. Moreno-Ramírez, A. Conde, Magnetocaloric effect: from materials research to refrigeration devices, Prog. Mater. Sci. 93 (2018) 112–232, https://doi.org/10.1016/j.pmatsci.2017.10.005.
[5] A. Biswas, A.K. Pathak, N.A. Zarkevich, X. Liu, Y. Mudryk, V. Balema, D.D. Johnson, V.K. Pecharsky, Designed materials with the giant magnetocaloric effect near room temperature, Acta Mater. 180 (2019) 341–348, https://doi.org/10.1016/j.actamat.2019.09.023.
[6] T. Krenke, E. Duman, M. Acet, E.F. Wassermann, X. Moya, L. Mañosa, A. Planes, Inverse magnetocaloric effect in ferromagnetic Ni–Mn–Sn alloys, Nat. Mater. 4 (6) (2005) 450–454, https://doi.org/10.1038/nmat1395.
[7] J.-H. Chen, T. Poudel Chhetri, A. Us Saleheen, D.P. Young, I. Dubenko, N. Ali, S. Stadler, Effects of heat treatments on magneto-structural phase transitions in MnNiSi-FeCoGe alloys, Intermetallics 112 (2019) 106547–106554, https://doi.org/10.1016/j.intermet.2019.106547.
[8] E. Liu, W. Wang, L. Feng, W. Zhu, G. Li, J. Chen, H. Zhang, G. Wu, C. Jiang, H. Xu, F. de Boer, Stable magnetostructural coupling with tunable magnetoresponsive effects in hexagonal ferromagnets, Nat. Commun. 3 (2012) 873, https://doi.org/10.1038/ncomms1868.
[9] Y. Kuang, B. Yang, X. Hao, H. Xu, Z. Li, H. Yan, Y. Zhang, C. Esling, X. Zhao, L. Zuo, Giant low field magnetocaloric effect near room temperature in isostructurally alloyed MnNiGe-FeCoGe systems, J. Magn. Magn. Mater. 506 (2020) 166782–166787, https://doi.org/10.1016/j.jmmm.2020.166782.
[10] A. Barcza, Z. Gercsi, K.S. Knight, K.G. Sandeman, Giant magnetoelastic coupling in a metallic helical metamagnet, Phys. Rev. Lett. 104 (24) (2010) 247202–247206, https://doi.org/10.1103/PhysRevLett.104.247202.
[11] T. Samanta, D.L. Lepkowski, A.U. Saleheen, A. Shankar, J. Prestigiacomo, I. Dubenko, A. Quetz, I.W.H. Oswald, G.T. McCandless, J.Y. Chan, P.W. Adams, D.P. Young, N. Ali, S. Stadler, Hydrostatic pressure-induced modifications of structural transitions lead to large enhancements of magnetocaloric effects in MnNiSi-based systems, Phys. Rev. B 91 (2) (2015) 020401–020406, https://doi.org/10.1103/PhysRevB.91.020401.
[12] Y. Song, S. Chen, S. Ma, Z. Zhang, K. Liu, S.U. Rehman, K. Yang, H. Zeng, Y. Zhang, C. Chen, X. Luo, Z. Zhong, Magneto-structural coupling through bidirectionally controlling the valence electron concentration in MnCoGe alloy, J. Magn. Magn. Mater. 495 (2020) 165865–165872, https://doi.org/10.1016/j.jmmm.2019.165865.
[13] P. Gębara, Z. Śniadecki, Structure, magnetocaloric properties and thermodynamic modeling of enthalpies of formation of (Mn,X)-Co-Ge (X = Zr, Pd) alloys, J. Alloys Compd. 796 (2019) 153–159, https://doi.org/10.1016/j.jallcom.2019.04.341.
[14] K. Synoradzki, Magnetocaloric effect in antiferromagnetic TmNiSn compound, J. Magn. Magn. Mater. 482 (2019) 219–223, https://doi.org/10.1016/j.jmmm.2019.03.064.
[15] T. Kanomata, H. Ishigaki, T. Suzuki, H. Yoshida, S. Abe, T. Kaneko, Magneto-volume effect of $MnCo_{1-x}Ge$($0 \leqslant x \leqslant 0.2$), J. Magn. Magn. Mater. 140-144 (1995) 131–132, https://doi.org/10.1016/0304-8853(94)00833-7.
[16] E.K. Liu, W. Zhu, L. Feng, J.L. Chen, W.H. Wang, G.H. Wu, H.Y. Liu, F.B. Meng, H.Z. Luo, Y.X. Li, Vacancy-tuned paramagnetic/ferromagnetic martensitic transformation in Mn-poor $Mn_{1-x}CoGe$ alloys, EPL 91 (1) (2010) 17003–17008, https://doi.org/10.1209/0295-5075/91/17003.
[17] S. Kaprzyk, S. Niziol, The electronic structure of CoMnGe with the hexagonal and orthorhombic crystal structure, J. Magn. Magn. Mater. 87 (3) (1990) 267–275, https://doi.org/10.1016/0304-8853(90)90759-J.
[18] G.J. Li, E.K. Liu, H.G. Zhang, Y.J. Zhang, J.L. Chen, W.H. Wang, H.W. Zhang, G.H. Wu, S.Y. Yu, Phase diagram, ferromagnetic martensitic transformation and magnetoresponsive properties of Fe-doped MnCoGe alloys, J. Magn. Magn. Mater. 332 (2013) 146–150, https://doi.org/10.1016/j.jmmm.2012.12.001.
[19] J.W. Lai, Z.G. Zheng, R. Montemayor, X.C. Zhong, Z.W. Liu, D.C. Zeng, Magnetic phase transitions and magnetocaloric effect of $MnCoGe_{1-x}Si_x$, J. Magn. Magn. Mater. 372 (2014) 86–90, https://doi.org/10.1016/j.jmmm.2014.07.035.
[20] L.F. Bao, F.X. Hu, R.R. Wu, J. Wang, L. Chen, J.R. Sun, B.G. Shen, L. Li, B. Zhang, X.X. Zhang, Evolution of magnetostructural transition and magnetocaloric effect with Al doping in $MnCoGe_{1-x}Al_x$ compounds, J. Phys. D 47 (5) (2014)https://doi.org/10.1088/0022-3727/47/5/055003.
[21] S.C. Ma, Y.X. Zheng, H.C. Xuan, L.J. Shen, Q.Q. Cao, D.H. Wang, Z.C. Zhong, Y.W. Du, Large room temperature magnetocaloric effect with negligible magnetic hysteresis losses in $Mn_{1-x}V_xCoGe$ alloys, J. Magn. Magn. Mater. 324 (2) (2012) 135–139, https://doi.org/10.1016/j.jmmm.2011.07.047.
[22] R.R. Wu, L.F. Bao, F.X. Hu, H. Wu, Q.Z. Huang, J. Wang, X.L. Dong, G.N. Li, J.R. Sun, F.R. Shen, T.Y. Zhao, X.Q. Zheng, L.C. Wang, Y. Liu, W.L. Zuo, Y.Y. Zhao, M. Zhang, X.C. Wang, C.Q. Jin, G.H. Rao, X.F. Han, B.G. Shen, Giant barocaloric effect in hexagonal Ni_2In-type Mn-Co-Ge-In compounds around room temperature, Sci. Rep. 5 (2015) 18027–18037, https://doi.org/10.1038/srep18027.
[23] Y. Li, H. Zhang, K. Tao, Y. Wang, M. Wu, Y. Long, Giant magnetocaloric effect induced by reemergence of magnetostructural coupling in Si-doped $Mn_{0.95}CoGe$ compounds, Mater. Des. 114 (2017) 410–415, https://doi.org/10.1016/j.matdes.2016.11.002.
[24] H. Imam, H.G. Zhang, W.J. Pan, B.T. Song, J.H. Shi, M. Yue, Magnetostructural transitions with a critical behavior in Y-doped MnCoGe compounds, Intermetallics 107 (2019) 53–59, https://doi.org/10.1016/j.intermet.2019.01.008.
[25] Y. Song, S. Ma, F. Yang, Z. Zhang, Y. Zhang, H. Zeng, S. Ur Rehman, G. Feng, X. Luo, C. Chen, Z. Lu, Z. Zhong, Co-vacancy induced magneto-structural transformation in co and Ge bidirectional-regulation MnCoGe systems, J. Alloys Compd. 819 (2020) 153061–153066, https://doi.org/10.1016/j.jallcom.2019.153061.
[26] S. Yang, Y. Song, X. Han, S. Ma, K. Yu, K. Liu, Z. Zhang, D. Hou, M. Yuan, X. Luo, C. Chen, Z. Zhong, Tuning the magnetostructural transformation in slightly Ni-substituted MnCoGe ferromagnet, J. Alloys Compd. 773 (2019) 1114–1120, https://doi.org/10.1016/j.jallcom.2018.09.266.
[27] C. Ma, Q. Ge, K. Liu, N. Ye, J. Tang, Microstructure, magnetic and magnetocaloric properties in magnetic-field-induced martensitic transformation $Mn_{1-x}Co_{1+x}Ge$ alloy ribbons, Phys. Lett. A 383 (18) (2019) 2223–2228, https://doi.org/10.1016/j.physleta.2019.04.028.
[28] A. Aryal, S. Pandey, I. Dubenko, D. Mazumdar, S. Stadler, N. Ali, Magnetostructural phase transitions and large magnetic entropy changes in Ag-doped $Mn_{1-x}Ag_xCoGe$ intermetallic compounds, MRS Commun. 9 (01) (2019) 315–320, https://doi.org/10.1557/mrc.2018.228.
[29] Q.Y. Ren, W.D. Hutchison, J.L. Wang, A.J. Studer, M.F. Md Din, S. Muñoz Pérez, J.M. Cadogan, S.J. Campbell, The magneto-structural transition in $Mn_{1-x}Fe_xCoGe$, J. Phys. D. Appl. Phys. 49 (17) (2016) 175003–175012, https://doi.org/10.1088/0022-3727/49/17/175003.
[30] S.C. Ma, D. Hou, C.W. Shih, J.F. Wang, Y.I. Lee, W.C. Chang, Z.C. Zhong, Magnetostructural transformation and magnetocaloric effect in melt-spun and annealed $Mn_{1-x}Cu_xCoGe$ ribbons, J. Alloys Compd. 610 (2014) 15–19, https://doi.org/10.1016/j.jallcom.2014.04.204.
[31] L. Caron, Z.Q. Ou, T.T. Nguyen, D.T. Cam Thanh, O. Tegus, E. Brück, On the determination of the magnetic entropy change in materials with first-order transitions, J. Magn. Magn. Mater. 321 (21) (2009) 3559–3566, https://doi.org/10.1016/j.jmmm.2009.06.086.
[32] T. Roisnel, J. Rodríquez-Carvajal, WinPLOTR: a windows tool for powder diffraction pattern analysis, Mater. Sci. Forum 378-381 (2001) 118–123, https://doi.org/10.4028/www.scientific.net/MSF.378-381.118.
[33] M.E. Wood, W.H. Potter, General analysis of magnetic refrigeration and its optimization using a new concept: maximization of refrigerant capacity, Cryogenics 25 (12) (1985) 667–683, https://doi.org/10.1016/0011-2275(85)90187-0.
[34] W.B. Pearson, The Crystal Chemistry and Physics of Metals and Alloys, Wiley-Interscience, New York, 1972.
[35] L. Caron, N.T. Trung, E. Brück, Pressure-tuned magnetocaloric effect in $Mn_{0.93}Cr_{0.07}CoGe$, Phys. Rev. B 84 (2) (2011) 020414–020418, https://doi.org/10.1103/PhysRevB.84.020414.
[36] W. Bażela, A. Szytula, J. Todorović, A. Zięba, Crystal and magnetic structure of the $NiMnGe_{1-n}Si_n$ system, Phys. Status Solidi (a) 64 (1) (1981) 367–378, https://doi.org/10.1002/pssa.2210640140.
[37] R. Kainuma, Y. Imano, W. Ito, Y. Sutou, H. Morito, S. Okamoto, O. Kitakami, K. Oikawa, A. Fujita, T. Kanomata, K. Ishida, Magnetic-field-induced shape recovery by reverse phase transformation, Nature 439 (7079) (2006) 957–960, https://doi.org/10.1038/nature04493.
[38] P. Shamba, J.L. Wang, J.C. Debnath, S.J. Kennedy, R. Zeng, M.F. Din, F. Hong, Z.X. Cheng, A.J. Studer, S.X. Dou, et al., J. Phys. Condens. Matter 25 (5) (2013) 056001–056008, https://doi.org/10.1088/0953-8984/25/5/056001.
[39] N.T. Trung, V. Biharie, L. Zhang, L. Caron, K.H.J. Buschow, E. Brück, From single- to double-first-order magnetic phase transition in magnetocaloric $Mn_{1-x}Cr_xCoGe$ compounds, Appl. Phys. Lett. 96 (16) (2010) 162507–162510, https://doi.org/10.1063/1.3399774.
[40] E. Brück, M. Ilyn, A.M. Tishin, O. Tegus, Magnetocaloric effects in $MnFeP_{1-x}As_x$-based compounds, J. Magn. Magn. Mater. 290-291 (2005) 8–13, https://doi.org/10.1016/j.jmmm.2004.11.152.

[41] A. Fujita, S. Fujieda, Y. Hasegawa, K. Fukamichi, Itinerant-electron metamagnetic transition and large magnetocaloric effects in $La(Fe_xSi_{1-x})_{13}$ compounds and their hydrides, Phys. Rev. B 67 (10) (2003) 104416–104428, https://doi.org/10.1103/PhysRevB.67.104416.

[42] A.O. Pecharsky, K.A. Gschneidner, V.K. Pecharsky, The giant magnetocaloric effect of optimally prepared $Gd_5Si_2Ge_2$, J. Appl. Phys. 93 (8) (2003) 4722–4728, https://doi.org/10.1063/1.1558210.

[43] A. Diestel, R. Niemann, B. Schleicher, S. Schwabe, L. Schultz, S. Fähler, Field-temperature phase diagrams of freestanding and substrate-constrained epitaxial Ni-Mn-Ga-Co films for magnetocaloric applications, J. Appl. Phys. 118 (2) (2015) 023908–023919, https://doi.org/10.1063/1.4922358.

[44] K.A. Gschneidner Jr., V.K. Pecharsky, A.O. Pecharsky, C.B. Zimm, Recent developments in magnetic refrigeration, Mater. Sci. Forum 315-317 (1999) 69–76, https://doi.org/10.4028/www.scientific.net/MSF.315-317.69.

[45] E. Brück, N.T. Trung, Z.Q. Ou, K.H.J. Buschow, Enhanced magnetocaloric effects and tunable thermal hysteresis in transition metal pnictides, Scripta Mater. 67 (6) (2012) 590–593, https://doi.org/10.1016/j.scriptamat.2012.04.037.

[46] J. Liu, Y. Gong, Y. You, X. You, B. Huang, X. Miao, G. Xu, F. Xu, E. Brück, Giant reversible magnetocaloric effect in MnNiGe-based materials: minimizing thermal hysteresis via crystallographic compatibility modulation, Acta Mater. 174 (2019) 450–458, https://doi.org/10.1016/j.actamat.2019.05.066.

[47] H. Zhang, Y. Li, E. Liu, K. Tao, M. Wu, Y. Wang, H. Zhou, Y. Xue, C. Cheng, T. Yan, K. Long, Y. Long, Multiple magnetic transitions in $MnCo_{1-x}Cu_xGe$ driven by changes in atom separation and exchange interaction, Mater. Des. 114 (2017) 531–536, https://doi.org/10.1016/j.matdes.2016.10.066.

[48] D. Choudhury, T. Suzuki, Y. Tokura, Y. Taguchi, Tuning structural instability toward enhanced magnetocaloric effect around room temperature in $MnCo_{(1-x)}Zn_{(x)}Ge$, Sci. Rep. 4 (2014) 7544–7550, https://doi.org/10.1038/srep07544.

[49] B.K. Banerjee, On a generalised approach to first and second order magnetic transitions, Phys. Lett. 12 (1) (1964) 16–17, https://doi.org/10.1016/0031-9163(64)91158-8.

[50] V. Franco, J. Blázquez, A. Conde, Field dependence of the magnetocaloric effect in materials with a second order phase transition: a master curve for the magnetic entropy change, Appl. Phys. Lett. 89 (22) (2006) 222512–222515, https://doi.org/10.1063/1.2399361.

[51] C.M. Bonilla, J. Herrero-Albillos, F. Bartolomé, L.M. García, M. Parra-Borderías, V. Franco, Universal behavior for magnetic entropy change in magnetocaloric materials: an analysis on the nature of phase transitions, Phys. Rev. B 81 (22) (2010) 224424–224431, https://doi.org/10.1103/PhysRevB.81.224424.

[52] A. Arrott, Criterion for ferromagnetism from observations of magnetic isotherms, Phys. Rev. 108 (6) (1957) 1394–1396, https://doi.org/10.1103/PhysRev.108.1394.

[53] L.A. Burrola-Gándara, C.R. Santillan-Rodriguez, F.J. Rivera-Gomez, R.J. Saenz-Hernandez, M.E. Botello-Zubiate, J.A. Matutes-Aquino, Comparison of the order of magnetic phase transitions in several magnetocaloric materials using the rescaled universal curve, Banerjee and mean field theory criteria, J. Appl. Phys. 117 (17) (2015) 17D144–17D149, https://doi.org/10.1063/1.4918340.

[54] J.Y. Law, V. Franco, L.M. Moreno-Ramirez, A. Conde, D.Y. Karpenkov, I. Radulov, K.P. Skokov, O. Gutfleisch, A quantitative criterion for determining the order of magnetic phase transitions using the magnetocaloric effect, Nat. Commun. 9 (1) (2018) 2680–2689, https://doi.org/10.1038/s41467-018-05111-w.

[55] C. Romero-Muniz, V. Franco, A. Conde, Two different critical regimes enclosed in the Bean-Rodbell model and their implications for the field dependence and universal scaling of the magnetocaloric effect, Phys. Chem. Chem. Phys. 19 (5) (2017) 3582–3595, https://doi.org/10.1039/c6cp06291a.

[56] V. Franco, A. Conde, M.D. Kuz'min, J.M. Romero-Enrique, The magnetocaloric effect in materials with a second order phase transition: Are T_C and T_{peak} necessarily coincident? J. Appl. Phys. 105 (7) (2009) 07A917–07A920, https://doi.org/10.1063/1.3063666.